IOPscience iopscience.iop.org

Home Search Collections Journals About Contact us My IOPscience

Magnetic exchange splitting in lanthanide metals

This article has been downloaded from IOPscience. Please scroll down to see the full text article.

2001 J. Phys.: Condens. Matter 13 11133

(http://iopscience.iop.org/0953-8984/13/49/303)

View the table of contents for this issue, or go to the journal homepage for more

Download details:
IP Address: 171.66.16.238
The article was downloaded on 17/05/2010 at 04:38

Please note that terms and conditions apply.

INSTITUTE OF PHYSICS PUBLISHING JOURNAL OF PHYSICS: CONDENSED MATTER

J. Phys.: Condens. Matter **13** (2001) 11133–11148 PII: S0953-8984(01)28231-9

Magnetic exchange splitting in lanthanide metals

Eugen Weschke and Günter Kaindl

Institut für Experimentalphysik, Freie Universität Berlin, Arnimallee 14, D-14195 Berlin, Germany

E-mail: eugen.weschke@physik.fu-berlin.de

Received 20 August 2001
Published 10 December 2001
Online at stacks.iop.org/JPhysCM/13/11133

Abstract

We report on a systematic study of the temperature dependences of the magnetic exchange splittings of two different valence states across the lanthanide series. Depending on the valence state, Stoner-like and spin-mixing behaviour are observed, with vanishing and persisting magnetic splitting, respectively, in the paramagnetic phases. The magnitudes of the splittings are found to scale linearly with the 4f spin moment, with no anomalies observed in antiferromagnetic phases. The results were obtained by means of angle-resolved photoemission from thin metal films grown epitaxially on W(110). The films were further characterized *in situ* in ultrahigh vacuum as regards their crystalline and magnetic structures using x-ray scattering and resonant magnetic x-ray diffraction, respectively.

1. Introduction

The electronic structure of lanthanide metals is a subject of continued interest, particularly in connection with their magnetic properties. Since the lanthanide metals exhibit a large variety of temperature-dependent magnetic structures including ferromagnetic, helical antiferromagnetic, and ferrimagnetic conical phases [1–4], a rather complex situation can be expected. The magnetic properties of the lanthanide metals are largely determined by the atomic-like 4f moments, which persist in the solid state [5]. Due to negligible 4f overlap between neighbouring sites, long-range magnetic order in lanthanide metals is induced by indirect magnetic exchange via conduction electrons, the so-called Ruderman–Kittel–Kasuya–Yosida (RKKY) interaction [6–8]. The RKKY coupling mechanism is particularly sensitive to details of the Fermi surface, and the relation of the periodicity of the magnetic structures to so-called nesting features is well established, both theoretically [2, 5] and experimentally [9, 10]. Most of the electronic structure studies carried out so far relate to the paramagnetic phases of the lanthanide metals; i.e., the influence of magnetic ordering and the particular magnetic structure on details of the temperature-dependent valence-electronic structure are largely unexplored. On the other hand, experimental techniques used for magnetism studies, such

 © 2001 IOP Publishing Ltd Printed in the UK

as the magneto-optical Kerr effect and resonant magnetic x-ray scattering techniques, involve the magnetic exchange splitting and spin polarization of the valence states and require a detailed understanding of their temperature dependences.

In the context of the relationship between electronic structure and magnetic ordering, the most studied lanthanide is Gd metal due to its role as a prototype local-moment ferromagnet [11–21]. The first observation of a temperature-dependent magnetic exchange splitting in Gd metal by means of angle-resolved photoemission (PE) was reported by Kim *et al* for the Δ_2 valence states [11]. This study revealed that the splitting vanishes at the bulk Curie temperature, T_C, closely following the magnetization. Resembling the characteristics of the valence states according to the Stoner model of band ferromagnetism [22–24], this behaviour is referred to as Stoner-like. It should be noted, however, that for a non-collinear magnetic structure, as in Gd metal at finite temperatures, the valence-electron spin is not a good quantum number and the notion of exchange splitting between majority- and minority-spin states in the sense of the Stoner model is therefore not correct [25]. This is due to the fact that the projection of a given valence state on the macroscopic 4f magnetization direction contains both spin directions, a feature that is often called spin mixing. Consequently, theoretical studies predict rather complex temperature dependences of magnetic exchange splitting and spin polarization besides the Stoner-like behaviour, including a persistent splitting above T_C [12–14, 25].

The search for pronounced spin-mixing behaviour and temperature-independent magnetic splitting raised some controversy, particularly in connection with the magnetic exchange splitting of the surface states on the close-packed surfaces of the trivalent lanthanide metals [15–19, 26]. Since the surface states are only partially occupied, they can be accessed neither by angle-resolved PE nor by inverse PE alone. The close proximity to the Fermi energy complicates the determination of their binding energies (BEs) by either of the two methods, and data suggesting Stoner-like [16, 17] as well as persistent splitting above T_C [15] were obtained. Particularly useful in this regard has been scanning tunnelling spectroscopy, which is capable of probing both occupied and unoccupied states in the vicinity of E_F in a single experiment. By this method, the surface states on Gd(0001) and Tb(0001) were shown to exhibit finite residual splittings above the highest magnetic ordering temperature, T^*, i.e., the Néel temperature T_N in the case of Tb [18, 19, 26, 27]. However, while for ferromagnetic Gd the splitting above T^* was found to be constant, a further decrease was observed in the case of Tb. This latter behaviour was explained by assuming persistence of temperature-dependent short-range antiferromagnetic correlations above T_N [26].

This contribution presents the results of systematic angle-resolved PE studies of the magnetic exchange splittings of two distinct valence states across the lanthanide series, revealing Stoner-like behaviour in one case and spin mixing in the other. The former is displayed by the above-mentioned Δ_2 states, which are the most pronounced bulk states in the PE spectra recorded from the close-packed surfaces of the trivalent lanthanide metals. The latter behaviour is observed for fully occupied surface states, which can be prepared by oxygen adsorption on these surfaces. The method of choice for studying magnetic exchange splitting was angle-resolved PE, which provides direct information on occupied electronic states. PE studies require very clean surfaces, which is a rather delicate issue in the case of the lanthanide metals. Therefore, the present studies were carried out on thin films grown on W(110) in ultrahigh vacuum (UHV), a method that has up to now provided the best samples in this respect. Besides the PE studies, the films were further characterized by means of x-ray scattering and resonant magnetic diffraction (XRD).

Employing these techniques, the experiments were carried out at different synchrotron radiation facilities. The angle-resolved PE studies were mainly performed at the Berliner Elektronenspeicherring für Synchrotronstrahlung (BESSY I) using a VSW ARIES

hemispherical electron energy analyser [21]. Additional PE experiments were carried out with a Scienta SES 200 analyser operated in angle-resolving mode and using 40.8 eV photons generated by a high-flux He resonance lamp selected by a grating monochromator. XRD and resonant magnetic XRD experiments were performed at the ID10 A beamline (Troïka) of the European Synchrotron Radiation Facility (ESRF) [28], utilizing a compact UHV chamber [29].

2. Sample preparation

2.1. Clean metal surfaces

PE and XRD studies were carried out in different experimental set-ups, with the samples, however, being prepared in an identical way *in situ* in UHV with base pressures of $<10^{-10}$ mbar. Gd, Tb, Dy, Ho and Lu metal films, with thicknesses between 100 Å and 300 Å, were deposited on W(110) at room temperature and subsequently annealed for a short time. 99.99% pure metals were evaporated from Ta crucibles heated by electron bombardment.

The trivalent heavy lanthanide metals grow in the form of close-packed planes of the hcp crystal structure on W(110). Accordingly, the films exhibit hexagonal low-energy electron diffraction (LEED) patterns with rather sharp spots that indicate well-ordered surfaces. This is in accordance with XRD results that establish high crystallinity throughout the entire films. To give an example, figure 1 displays the specular reflectivity of a 77 Å thick Ho film as a function of the scattering vector q, given in units of the (non-primitive) reciprocal-lattice parameter c^* of the hcp lattice of Ho. The Bragg peak corresponding to diffraction by the close-packed planes occurs at $q = 2c^*$. The reflectivity curve displays oscillations at low scattering vectors, the so-called Kiessig fringes [30, 31]. These oscillations are well resolved, indicating homogeneous film thickness and rather small roughnesses both at the surface and at the film/substrate interface [31]. Due to the finite number of layers contributing to the coherent diffraction signal, the (002) Bragg reflection does not consist of a single sharp peak but instead

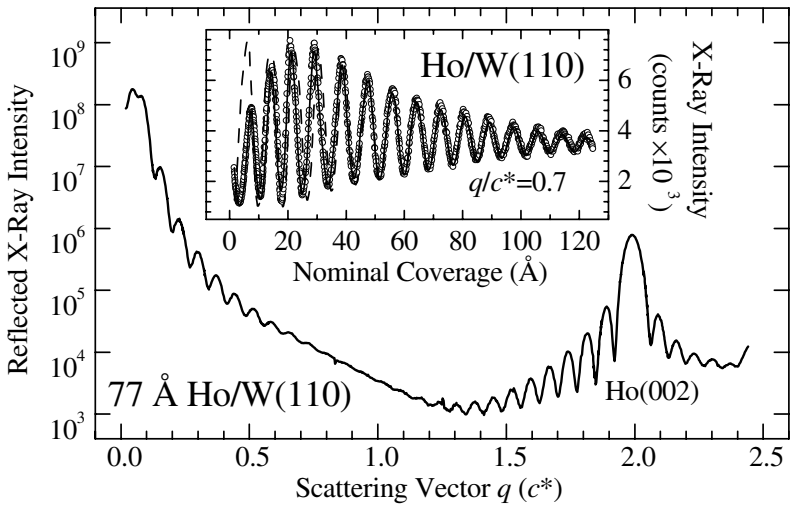

Figure 1. Specular x-ray reflectivity of a 77 Å thick Ho film grown on W(110), recorded with a photon energy of 8074 eV. The inset displays oscillations of the x-ray reflectivity at a fixed scattering vector during the growth of Ho on W(110).

exhibits pronounced side maxima, the so-called Laue oscillations [32]. The periods of the Kiessig fringes and of the Laue oscillations are identical, establishing crystalline coherence of the close-packed layers across the whole film. The transverse width measured at the (002) Bragg peak is $\approx 0.04^\circ$, which comes close to the mosaic spreads of high-quality bulk single crystals [33].

The inset in figure 1 displays the x-ray reflectivity recorded at a fixed scattering vector of $q = 0.7c^*$ during the growth of Ho on W(110). Due to the rather well-defined layer-by-layer growth, pronounced oscillations in the reflected intensity were observed [29]. These oscillations are essentially determined by the interference of x-rays scattered from the film surface and the film/substrate interface, since in the case of hard x-rays, the penetration depth is large compared to the film thickness during the whole growth process. The growth–oscillation period does not correspond to a single atomic layer, but exhibits a distinct dependence on the scattering vector in the case of heteroepitaxy [29]. At film thicknesses exceeding $\approx$30 Å, the oscillations are regular, with decreasing amplitudes due to increasing film roughness. In the initial stages of deposition, both the phases and the amplitudes of the oscillations behave irregularly, which provides detailed information on the dynamics of the growth process, since these irregularities are due to the relaxation during the growth of film layers close to the substrate [29, 34].

Epitaxial lanthanide metal films grown in this way exhibit very clean surfaces with no contamination detectable by means of surface-sensitive PE [35]. This is shown in figure 2 for the example of an epitaxial Gd metal film. The bottom spectrum was recorded directly after deposition at low temperatures, i.e., from a strongly disordered film. Accordingly, the 4f-spectral features around 8.5 eV binding energy (BE) are rather broad and the emission from valence states in the vicinity of the Fermi energy E_F contains contributions from various parts of the Brillouin zone. Note the absence of any features around 6 eV and 4 eV BE, which would indicate the presence of oxygen or hydrogen, respectively [36, 37].

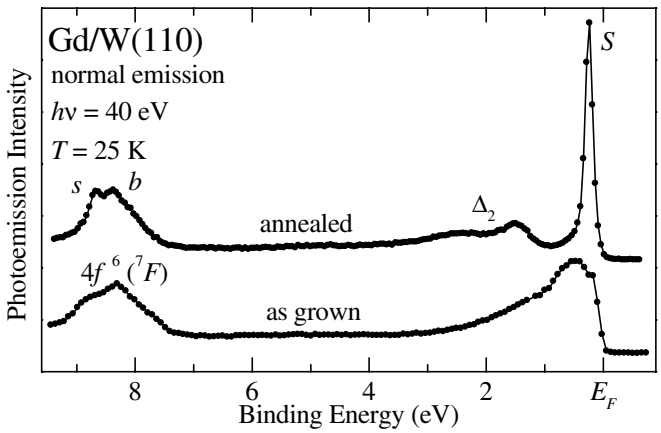

Figure 2. Angle-resolved photoemission spectra recorded in normal-emission geometry from an $\approx$100 Å thick Gd film directly after deposition on W(110) at 25 K (bottom) and upon annealing at 700 K for $\approx$5 seconds (top).

Upon annealing, all features sharpen substantially, as seen in the top spectrum of figure 2. The 4f features exhibit two well-resolved components due to emission from atoms in the bulk (b) and in the topmost surface layer (s), separated by a surface core-level shift (SCS) of $\approx$290 meV [38]. The valence-band emission displays three distinct features. Two broad peaks

at a BE of ≈2 eV are due to emission from the Δ_2 bulk band states [11], split into majority and minority components at low temperatures [11, 39]. The most pronounced feature in the top spectrum of figure 2 close to E_F is due to emission from the surface state S, a common feature of all close-packed surfaces of the trivalent lanthanide metals [40]. While the Δ_2 states are fully occupied, the minority component of the surface state is located well above the Fermi energy and is hence not accessible to PE. It turns out, however, that a fully occupied magnetic surface state can be prepared on the close-packed lanthanide surfaces by adsorption of a monolayer of oxygen [41–43].

2.2. Surface oxides

Dosing ≈1 Langmuir (10^{-6} Torr s) of molecular oxygen onto the close-packed surfaces of the trivalent heavy lanthanide metals at room temperature and subsequent annealing leads to the formation of well-ordered adsorbate systems. The annealing temperature is limited by the onset of oxygen desorption, occurring at ≈350 K in the case of Gd, but not below 700 K in the case of Lu. These oxygen adsorbate systems are well ordered, exhibiting sharp (1×1) LEED patterns.

However, the adsorption of oxygen does not yield the trivalent sesquioxides Ln_2O_3, which are the well-known stable bulk compounds. Instead, the adsorbate phases are characterized by rather different electronic structures, as shown in figures 3 and 4 for the examples of Lu and Gd, respectively. The right-hand panel of figure 3 displays angle-resolved PE spectra of an almost clean Lu film, upon oxygen adsorption and subsequent annealing, and of a thin film of the sesquioxide Lu_2O_3, recorded at $h\nu = 40$ eV. At this photon energy, the latter two spectra are dominated by emission from O 2p states. While the Lu_2O_3 spectrum is characterized by a broad multi-component feature, the adsorbate phase exhibits a rather sharp peak at ≈6 eV BE. The lower two spectra of the right-hand panel in figure 3 indicate substantial changes in the valence-band region upon oxygen adsorption. The surface state S is essentially suppressed, while a new peak S_2 is observed around 1 eV BE, which turns out to represent an oxygen-induced surface state characteristic of all lanthanide metals of the present study. It should be noted that Lu_2O_3 does not display any PE intensity in the region of the Fermi energy, as expected for an insulating oxide.

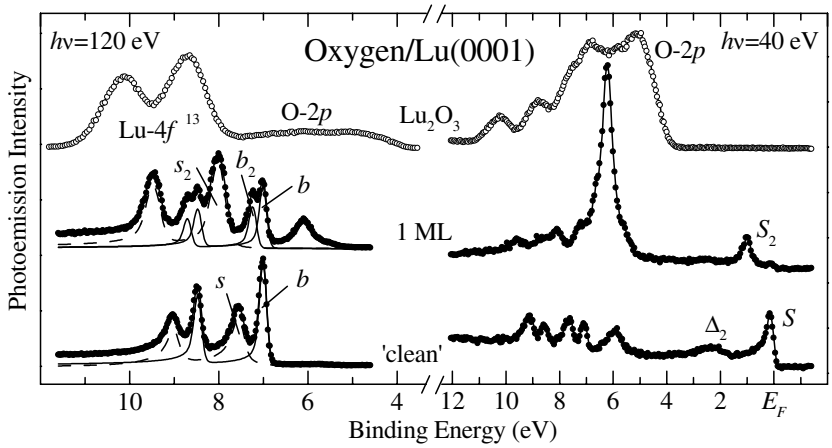

Figure 3. Angle-resolved photoemission spectra recorded in normal-emission geometry from Lu metal (bottom spectra), after preparation of the surface oxide, and from Lu_2O_3.

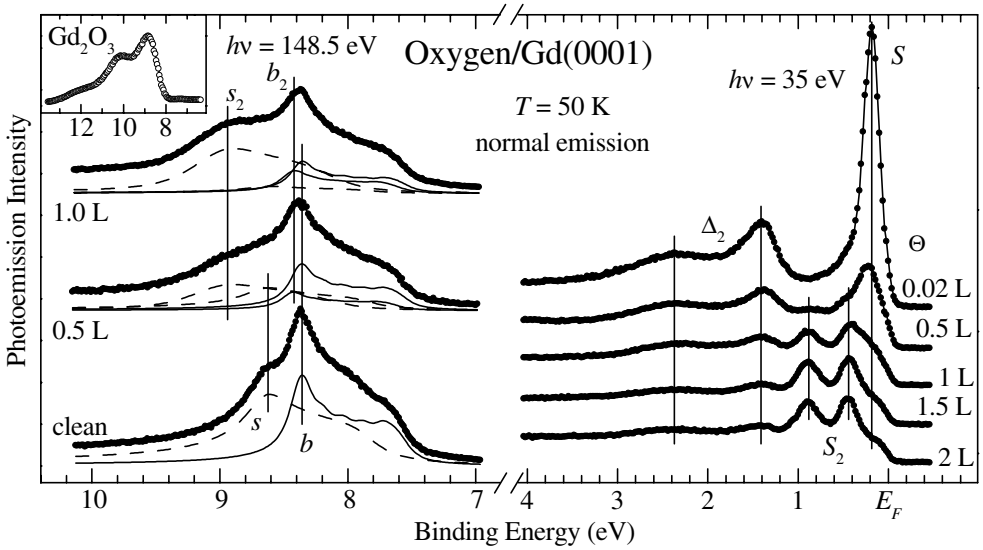

Figure 4. Photoemission spectra of Gd(0001) at various stages of oxygen exposure Θ. Left panel: 4f spectra recorded at the maximum of the 4d → 4f resonance. The inset shows a corresponding spectrum recorded from a thin film of the sesquioxide Gd_2O_3. Right panel: angle-resolved photoemission spectra illustrating the concomitant changes in the vicinity of the Fermi energy.

The distinct difference between the oxygen adsorbate phase and the sesquioxide is also reflected in the 4f spectra of the left panel, recorded at $h\nu = 120$ eV. At this photon energy, the PE cross section of 4f states is large. Hence the 4f-spectral features can be clearly distinguished from the otherwise dominating O 2p emission. Lu metal with a fully occupied 4f shell in the ground state exhibits a $4f^{13}$ final-state doublet with well-resolved bulk (b) and surface (s) components. Upon adsorption of oxygen, s is completely suppressed. Two new components, labelled b_2 and s_2 are observed, which can be assigned to Lu subsurface and surface atoms, respectively [41]. In the case of s_2, the chemical shift with respect to s has a comparably large value of 470 ± 50 meV. This characterizes the adsorption process as chemisorption rather than weak physisorption [44, 45], supporting the notion of a surface oxide. The 4f spectrum of the surface oxide, characterized by emission from three Lu species with well-defined chemical environments, is distinctly different from that of the single broad doublet of Lu_2O_3.

The reaction of oxygen with the close-packed surfaces of trivalent lanthanide metals is confined to the topmost layer and affects the surface and the subsurface layers only, with negligible diffusion of oxygen into the bulk. This can be inferred from the left panel of figure 4, which displays 4f PE spectra recorded from the clean Gd(0001) surface and after two steps of oxygen adsorption. The spectra were recorded with a photon energy of 148.5 eV, corresponding to the maximum of the 4d → 4f resonance, where the 4f PE cross section is most strongly enhanced. This allows a detailed analysis of the 4f spectra without interfering contributions from O 2p emission. The spectra can be decomposed in terms of the four different contributions already observed in the spectra of figure 3. The spectrum of the clean film (bottom) consists of b and s (cf. figure 2). Upon oxygen adsorption, the intensity of s decreases, being balanced by the increase of s_2. This behaviour characterizes the adsorption of oxygen as a pure surface reaction with negligible diffusion of oxygen into the bulk of the film. The decrease of b is balanced by the increase of b_2, which is not as well resolved here as in the

case of Lu. Nevertheless, it can be distinguished as a shoulder to *b* in the top spectrum, and its contribution is necessary for a consistent description of the spectra in figure 4. Again, the 4f PE spectrum of the surface oxide is different from that of the sesquioxide Gd_2O_3, displayed in the inset of the left panel.

The right panel of figure 4 displays angle-resolved PE spectra in the vicinity of the Fermi energy at various stages of oxygen adsorption, recorded in normal-emission geometry with a photon energy of 35 eV. While all of the spectra were recorded at low temperatures, the film was annealed to 345 K after each exposure step in order to provide well-ordered surfaces. These spectra provide a detailed overview on the concomitant changes in the valence-electronic structure. The top spectrum displays the same valence-band features as shown in figure 2. With increasing oxygen dosage, the intensity of the surface state *S* decreases, while *two* new features S_2 develop in the Gd case, in contrast to the single peak of non-magnetic Lu (cf. right panel of figure 3). These two S_2 features are assigned to the exchange-split components of an oxygen-induced surface state. The surface-related character of S_2 can be inferred from the fact that the reaction of oxygen occurs only at the surface. It is further corroborated by the lack of dispersion upon changing the photon energy, i.e., the electron momentum perpendicular to the surface, as expected for a two-dimensional electronic state [42]. Obviously, this oxygen-induced surface state—unlike *S*—is fully occupied, with both exchange-split components accessible to PE investigations.

In the following, the temperature dependences of the magnetic splittings of both the Δ_2 states and S_2 will be discussed on the basis of a systematic study across the lanthanide series. Before turning to this discussion, however, another important aspect in the present context is addressed, namely whether the bulk magnetic structures of the lanthanide metals persist in thin films grown on W(110).

3. Magnetic structure of thin lanthanide metal films on W(110)

As mentioned in the introduction, epitaxial lanthanide metal films grown *in situ* in UHV constitute the preferred samples for PE studies. For such thin films, however, the persistence of the bulk magnetic properties cannot be anticipated. Since the magnetic structures of the lanthanide metals are determined by a delicate temperature-dependent balance between RKKY interaction and magnetostrictive energies as well as crystalline anisotropy [5, 46], modifications can be expected to occur in thin films due to the influence of interfaces. This has been observed, e.g., for Dy superlattices, where either ferromagnetic or helical phases can be suppressed, depending on the strain induced by the respective adjacent layers [46, 47]. Therefore, an interpretation of the PE data in connection with the magnetic structures requires further characterization of the films, which was achieved here by employing the method of magnetic XRD.

Up to the present work, studies of thin-film magnetic structures by means of magnetic neutron or x-ray diffraction have been carried out on *ex situ* prepared samples capped by protective layers. Such cap layers, on the other hand, can alter the magnetic structure. It is therefore mandatory to characterize the same films as are studied using PE, an undertaking that has only recently been achieved by *in situ* resonant magnetic XRD in the cases of Ho metal [21] and Dy metal [48].

With the availability of high-intensity x-ray beams at synchrotron radiation facilities, magnetic XRD applied in the study of magnetic structures has become a competitive method. Although the magnetic scattering cross section is usually smaller by orders of magnitude than that of charge scattering [49], an improved contrast between magnetic and charge scattering can be obtained by employing a polarization analysis of the scattered x-rays. This exploits

the fact that the magnetic scattering process involves a rotation of the x-ray polarization by 90°, which is not the case for charge scattering. With incoming σ-polarized x-rays, magnetic contributions can be distinguished in the π-polarization channel of the scattered intensity [50].

Magnetic scattering can be further enhanced by tuning the photon energy to a core-excitation resonance. Depending on the exchange splitting and the spin polarization of the unoccupied states involved in the resonance excitation, a substantial increase of the magnetic scattering cross section can be achieved [51], ranging from ≈50 at lanthanide L_3 edges [52] to several orders of magnitude at lanthanide M_5 edges that involve dipole transitions into the 4f states [53].

The magnetic XRD method can be readily applied to antiferromagnetic systems, since magnetic superstructure diffraction peaks and those from charge scattering are usually well separated in momentum space. For thin films, however, additional difficulties occur. To begin with, the number of scatterers and, hence, the total scattered intensity are strongly reduced. In addition, diffraction features are no longer single narrow peaks but are spread over a larger region in momentum space (cf. figure 1), which gives rise to a strong charge background at the position of the main maximum of the magnetic superstructure reflection.

This is illustrated in figure 5 for the case of Ho metal, characterized by a helical antiferromagnetic structure over a wide temperature range between ≈20 K and the Néel temperature $T_N \approx 131$ K. In this structure, the 4f moments are ferromagnetically ordered in the close-packed planes and the magnetic moments form a helix along the c-axis of the hcp lattice. The helix period is ≈10 ML at 40 K [33], corresponding to a wave vector of $\tau \approx 0.2c^*$. The data of figure 5 were recorded at $h\nu = 8074$ eV, corresponding to the maximum of the L_3 resonance. The top curve displays the specular reflectivity of a 113-monolayer-thick Ho film around the (002) Bragg peak recorded in the $\sigma\sigma$-channel. Here, the magnetic superstructure peaks are concealed by the Laue oscillations of the chemical Bragg peak. A contrast is obtained, however, when the reflected x-ray intensity is detected in the π-channel, as seen in the bottom curve of figure 5. In this case, the charge scattering is suppressed by a factor of ≈500, and the magnetic superstructure peaks are clearly visible. Thus, the temperature-dependent magnetic structure of a Ho film 113 ML thick can be readily characterized, as shown in the inset. The

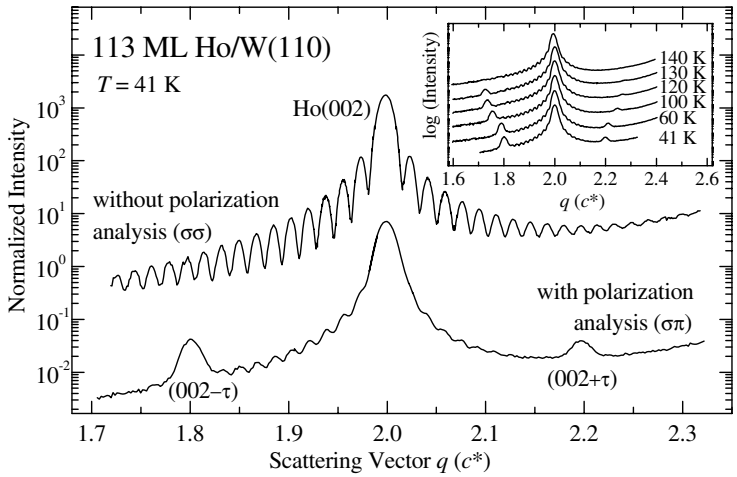

Figure 5. Resonant magnetic XRD at the L_3 absorption edge from a Ho film 113 ML thick, demonstrating the magnetic contrast enhancement by polarization analysis. The inset shows the temperature dependence of the magnetic superstructure satellite.

intensities and the positions of the magnetic satellites as a function of temperature are found to be the same as for bulk Ho (cf. figure 11, later) [21], demonstrating that for thin Ho films on W(110) the bulk magnetic structure persists at least down to this thickness. Similarly, the well-known helical magnetic structure of Dy metal in the antiferromagnetic phase has recently also been observed for thin Dy films grown on W(110) [48].

A characterization of even thinner films by means of magnetic XRD gets more and more demanding. With hard x-rays at the Ho L_3 edge, the limit for thin-film studies has been found to be of the order of 30 ML [54]. This limit, however, has recently been lowered by the resonant magnetic x-ray diffraction at the Ho M_5 edge. By an increase of the magnetic scattering cross section by several orders of magnitude, the sensitivity is increased to permit studies at least down to $\approx$10 monolayers [53].

Having established that the bulk magnetic structure of Ho metal persists in thin epitaxial films on W(110) at least down to 113 monolayers, a consideration of the magnetic exchange splitting in connection with the helical antiferromagnetic structure is possible.

4. Temperature dependence of magnetic exchange splitting

The observation of a Stoner-like magnetic splitting of the Δ_2 states in Gd metal [11] initiated a number of theoretical studies of the temperature-dependent electronic structure of local-moment magnetic systems [12–14, 25].

Nolting *et al* applied a many-body approach to calculate the magnetic splitting and spin polarization of various valence states, using a phenomenological temperature-dependent 4f magnetization [13, 14]. Considering two extreme cases, itinerant s-like states at higher BEs were found to be sensitive to long-range magnetic order, with an energy splitting that essentially reflects the net magnetization and hence vanishes at the Curie temperature, T_C. In contrast, the splitting of more localized d-like states in the vicinity of the Fermi energy, E_F, depends only on the temperature-independent local 4f moment and was hence found to be essentially temperature independent, persisting in the paramagnetic phase. For various states within the band structure, usually a mixture of these two limiting cases was found.

The influence of the temperature-dependent magnetic order on the band structure of Gd was also studied by Sandratskii and Kübler using a model that allows a finite angle between the 4f moments in adjacent close-packed layers [12, 25]. In this model, the 4f magnetic structure can form a helix along the crystallographic *c*-axis of hcp Gd. This structure imposes a generalized translational symmetry, which allows a calculational treatment. In this model, the fully ordered ferromagnetic phase at zero kelvins is reproduced by an infinite helix period, while increasing temperatures are simulated by a decreasing helix period. The results obtained with this model resemble those of Nolting *et al*, revealing a complex temperature-dependent redistribution of minority- and majority-spin contributions in the valence band. Also in these calculations, states at higher BEs were found to show Stoner-like behaviour [12]. Interestingly, substantial magnetic splitting is observed down to a helix period of $\approx$4 monolayers [12]. Since the model used by Sandratskii and Kübler reproduces exactly the magnetic structure of Ho, magnetic exchange splitting can be expected in the helical antiferromagnetic phase despite the zero net magnetization.

4.1. Stoner-like behaviour: Δ_2 bulk states

The Stoner-like temperature dependence of the Δ_2 splitting was originally interpreted as reflecting the macroscopic magnetization [11]; the behaviour of the exchange splitting in antiferromagnetic lanthanide metals, however, reveals that this is not necessarily true [21].

Figure 6 displays angle-resolved PE spectra of Gd, Ty, Dy and Ho, recorded with a photon energy of 35 eV that corresponds to an initial-state electron wave vector close to the Γ_4 point of the Brillouin zone [11]. The spectra were recorded at temperatures well below the respective highest magnetic ordering temperatures. At the given temperatures, Gd, Tb and Dy are ferromagnetic, while the Ho film is in the helical antiferromagnetic phase, as verified by magnetic x-ray diffraction. All metals show magnetic splitting, which decreases from Gd to Ho. In the case of Ho, the splitting is not as well resolved as in the other cases; nevertheless, a shoulder can be clearly distinguished.

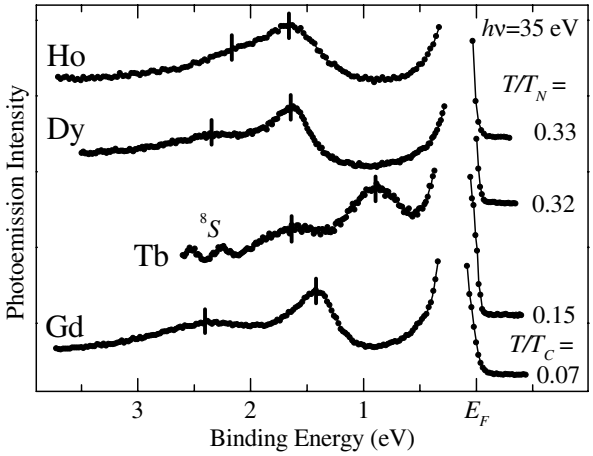

Figure 6. Angle-resolved PE spectra recorded in normal-emission geometry (except for Tb) from the (0001) surfaces of the given heavy lanthanide metals. In order to avoid an overlap with the ^8S multiplet component of the 4f emission, the Tb spectrum was recorded at an emission angle of 8° off normal; in this way the Δ_2 emission was shifted to lower BE. In normal emission, $h\nu = 35$ eV corresponds to an initial-state electron wave vector close to the Γ_4 critical point.

An overview of temperature-dependent PE spectra of the four lanthanide metals studied is given in figure 7, revealing a rather systematic behaviour with a Stoner-like decrease of the magnetic splitting up to the respective highest magnetic ordering temperature in each case. The spectra were analysed using two symmetric Lorentzian-shaped components for the Δ_2 states and an additional component for the surface state S; a triangular background as observed for polycrystalline films (cf. figure 2) was used to account for contributions from other parts of the Brillouin zone. In this way, consistent fits of all of the spectra in figure 7 were obtained.

The essential results of these fits are shown in figure 8. The left panel displays the reduced magnetic splittings $\Delta E(T)/\Delta E(0)$ plotted versus the reduced temperature T/T^*, where T^* denotes the respective highest magnetic ordering temperature of each lanthanide metal. The Δ_2 states of all lanthanides exhibit the same Stoner-like behaviour, with the magnetic exchange splittings essentially vanishing in the paramagnetic phases. The right panel of figure 8 displays the zero-temperature splittings $\Delta E(0)$ readily obtained by extrapolation; it establishes that the magnetic exchange splittings depend linearly on the 4f spin moment. While such a scaling has been anticipated for the lanthanide metals [55, 56], the present data represent a direct experimental observation. Figure 8 demonstrates that the relevant temperature scale for the magnetic splitting is not given by the ferromagnetic ordering temperature T_C but instead by the highest magnetic ordering temperature T^*. Furthermore, no anomaly has been observed in the antiferromagnetic phases, with the splitting not even being reduced in Ho, despite the vanishing net magnetization.

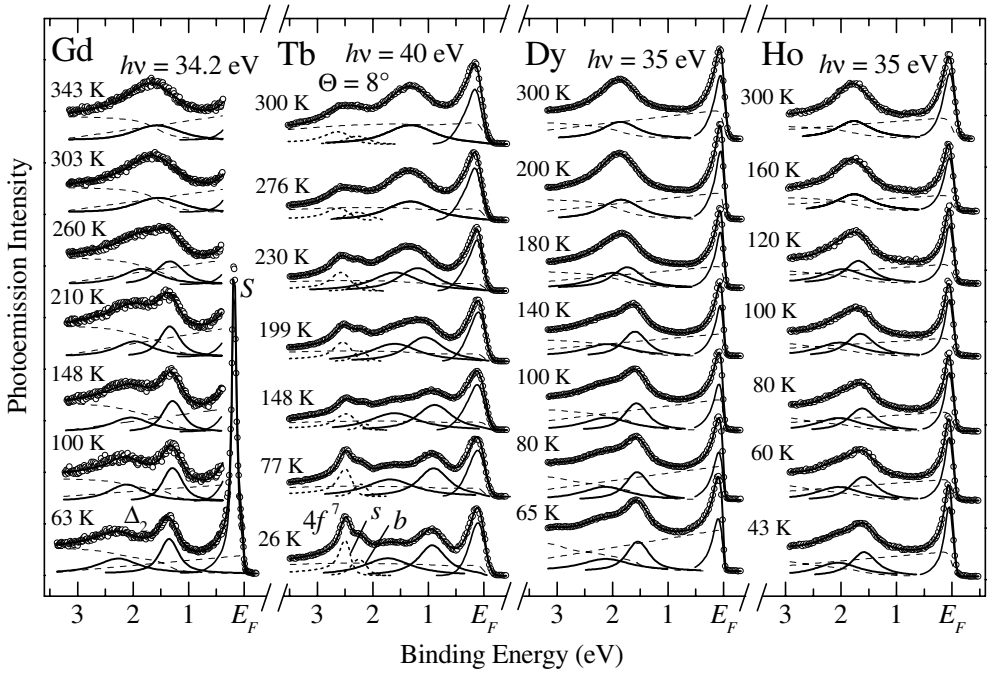

Figure 7. Temperature-dependent angle-resolved photoemission spectra of Gd, Tb, Dy and Ho in normal-emission geometry.

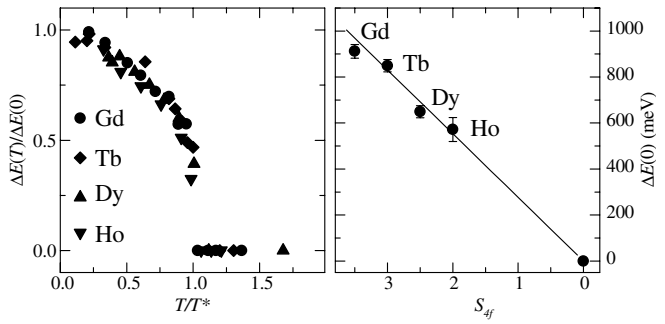

Figure 8. Left panel: temperature dependences of the magnetic splittings $\Delta E(T)$ of the Δ_2 states of Gd, Tb, Dy and Ho normalized to the respective zero-temperature splittings $\Delta E(0)$. Right panel: $\Delta E(0)$ versus 4f spin moment; the solid line represents a linear fit.

This latter result shows that the magnetic exchange splitting of Δ_2 band states, albeit exhibiting Stoner-like temperature dependence, does not necessarily reflect the macroscopic magnetization of the system. A consistent picture for the Stoner-like temperature dependence of the Δ_2 splitting *and* its scaling with the full 4f spin moment in the helical phase can be obtained by assigning the magnetic splitting of the Δ_2 states, at least in Ho metal, to the magnetization of a magnetic subsystem, namely the ferromagnetically ordered close-packed (0001) planes. In this case, the relevant temperature would be T_N rather than T_C. Such a behaviour can be explained by assuming a wave function with considerable itineracy in the basal plane and a higher degree of localization with respect to the c-axis direction [21].

4.2. Magnetic splitting of oxygen-induced surface states

While the Δ_2 band states exhibit essentially a Stoner-like temperature dependence of the magnetic splitting, characteristics of spin-mixing behaviour are observed for the oxygen-induced surfaces states described above.

Figure 9 gives an overview of temperature-dependent PE spectra, recorded from the surface oxides of Gd, Tb, Dy and Ho and, for comparison, also Lu. The best-resolved magnetic splitting of the oxygen-induced surface state s_2 is observed in the case of Gd at low temperatures; this splitting decreases with increasing temperature. In contrast to the case for the Δ_2 band states, however, the splitting clearly remains finite even above the Curie temperature of Gd ($T_C = 293$ K), as can be inferred from the asymmetry of the high-temperature spectra. As in the case of the Δ_2 band states, the splitting decreases with decreasing 4f spin moment, behaving in an analogous systematic way. Also in this case, a consistent fit analysis of the PE spectra could be carried out, using two symmetric Lorentzians to describe S_2. It is important to note that the spectra of non-magnetic Lu can be readily described by a single symmetric line for all temperatures. This supports the interpretation of the spectra of the magnetically ordered lanthanide metals in terms of magnetic splitting and further demonstrates that a finite splitting persists in the paramagnetic phases of these lanthanides.

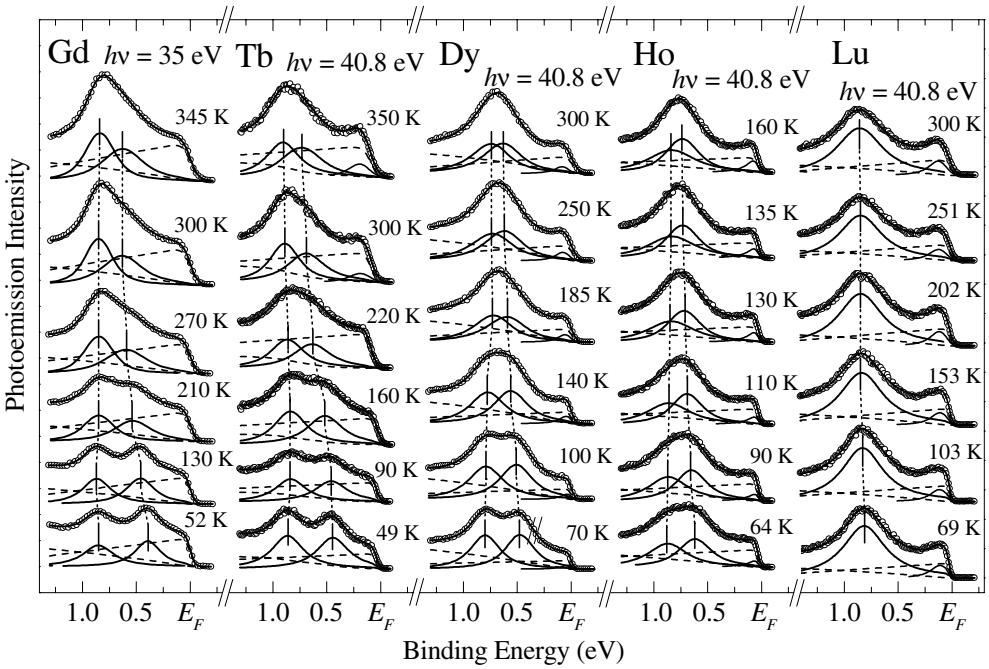

Figure 9. Temperature-dependent angle-resolved photoemission spectra recorded from the surface oxide phases of Gd, Tb, Dy and Ho in normal-emission geometry.

The results of the fit analyses are shown in figure 10, revealing a systematic behaviour also in the case of the oxygen-induced surface states. The left panel shows that the magnetic splittings, despite decreasing with increasing temperature, persist in the paramagnetic phases above the respective highest magnetic ordering temperatures. Such a behaviour is typical for states with pronounced spin mixing [14], which hence can be assigned to the oxygen-induced surface states, although no spin analysis was performed in the present study.

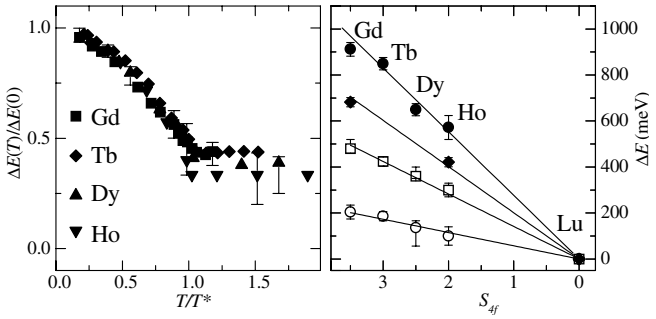

Figure 10. Left panel: temperature dependence of the magnetic splittings $\Delta E(T)$ of the oxygen-induced surface states on Gd, Tb, Dy and Ho normalized to the respective zero-temperature splittings $\Delta E(0)$. Right panel: zero-temperature splittings (open squares) and residual splittings above T^* of oxygen-induced surface states (open circles). For comparison, the zero-temperature Δ_2 splittings (solid circles) and the splittings of the surface state on clean surfaces (solid diamonds; from tunnelling spectroscopy [27]) are included.

The right panel of figure 10 summarizes the scaling behaviour of the various splittings, including the zero-temperature splittings of the Δ_2 band states (solid circles) and of the surface states S of the clean lanthanide metal surfaces (solid diamonds). The figure demonstrates that all splittings depend linearly on the 4f spin moment. In the case of the oxygen-induced surface states, this is true for the zero-temperature splittings (open squares) as well as for the persisting splittings above T^* (open circles). This indicates that the persisting splittings in the paramagnetic phase of states with pronounced spin-mixing behaviour are indeed caused by the local exchange interaction with 4f spin moments even in the absence of long-range magnetic order. The magnitudes of the splittings depend on the strength of the local exchange interaction. They are largest for Δ_2 band states, while they are distinctly smaller in the case of S_2. This is in accordance with S_2 containing substantial admixture of O 2p states [42, 43] that reduces the overlap at the 4f site.

5. Conclusions

In this contribution, a systematic study of magnetic exchange splitting in the lanthanide metals was presented for the example of two distinct valence states, the Δ_2 bulk band states and the oxygen-induced surface states. In accordance with theoretical considerations, it was found that the splitting does not necessarily reflect the macroscopic magnetization, but may depend in a more complicated way on the magnetization of a subsystem or even on the size of the local 4f magnetic moment only.

While this was shown here for two particular states, similar complexities can be expected in other parts of the Brillouin zone, depending on the correlation length of the corresponding wave function. In the case of unoccupied states in the vicinity of E_F, this may have important implications for resonant magnetic XRD. The square root of the integrated magnetic satellite intensity (figure 5) is generally used as a measure of the order parameter of the helical phase, the so-called staggered magnetization [33]. While this is true for non-resonant magnetic x-ray scattering studies, resonant magnetic XRD at the $L_{2,3}$ edges involves transitions into unoccupied 5d states and may hence turn out to be more complicated. Thus, changes in the 5d band polarization have been considered to account for an unusual temperature dependence of the L_3/L_2 branching ratio in $DyFe_4Al_8$ [57].

Along these lines, an interesting observation can be made by comparing the magnetic exchange splitting of Δ_2 band states with the temperature dependence of the square roots of the intensities of the magnetic $(0\,0\,2-\tau)$ satellite in Ho metal, as shown in figure 11. The latter (open circles) can be essentially described by a power law, using the bulk values of the critical exponent $\beta = 0.39$ and of $T_N = 131.4$ K (solid line) [33]. The magnetic exchange splittings (solid squares), on the other hand, display a similar behaviour, suggesting that both reflect the same quantity, namely the ferromagnetic order of the close-packed (0001) planes. On the basis of the present data, which still show substantial scatter, this is rather speculative. It is interesting to note, however, that the temperature dependence of the magnetic satellite intensity of Ho is not fully understood since the corresponding critical exponent β, based on resonant magnetic XRD results, does not exhibit a mean-field scaling; in addition, the universality class of the helical antiferromagnets is still unclear [4].

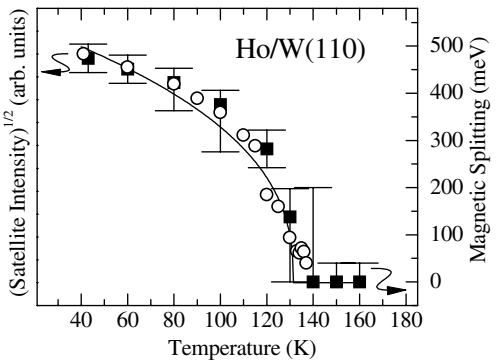

Figure 11. Temperature dependences of the Ho Δ_2 splitting (solid squares) and of the square root of the integrated $(0\,0\,2-\tau)$ magnetic XRD intensity (open circles). The solid curve represents a power-law dependence with bulk $T_N = 131.4$ K and critical exponent $\beta = 0.39$ [33].

Acknowledgments

The authors gratefully acknowledge various contributions of present and previous members of their research group at the Freie Universität Berlin, in particular by C Schüßler-Langeheine, R Meier, H Ott, Chandan Mazumdar, A Yu Grigoriev, D V Vyalikh, L Kilian, and A Möller. The x-ray results were obtained in close collaboration with C Sutter and G Grübel of the European Synchrotron Radiation Facility. Stimulating discussions with W Nolting and P J Jensen are acknowledged. This work was financially supported by the Bundesministerium für Bildung und Forschung, projects 05-625 KEC and 05 SF8 KEC8, as well as the Deutsche Forschungsgemeinschaft, Sfb-290/TPA06 and Ka-564/2.

References

[1] Sinha S K 1978 *Handbook on the Physics and Chemistry of Rare Earths* vol 1, ed K A Gschneidner Jr and L Eyring (Amsterdam: North-Holland)
[2] Koehler W C 1972 *Magnetic Properties of Rare Earth Metals* ed R J Elliott (London: Plenum)
[3] Gibbs D, Moncton D E, D'Amico K L, Bohr J and Grier B H 1985 *Phys. Rev. Lett.* **55** 234
[4] Helgesen G, Hill J P, Thurston T R and Gibbs D 1995 *Phys. Rev.* B **52** 9446
[5] Jensen J and Macintosh A R 1991 *Rare Earth Magnetism* (Oxford: Clarendon)
[6] Ruderman M A and Kittel C 1954 *Phys. Rev.* **96** 99

[7] Kasuya T 1956 *Prog. Theor. Phys.* **16** 45
[8] Yosida K 1957 *Phys. Rev.* **106** 893
[9] Dugdale S B, Fretwell H M, Alam M A, Kontrym-Sznajd G, West R N and Badrzadeh S 1997 *Phys. Rev. Lett.* **79** 941
[10] Fretwell H M, Dugdale S B, Alam M A, Hedley D C R, Rodriguez-Gonzalez A and Palmer S B 1999 *Phys. Rev. Lett.* **82** 3867
[11] Kim B, Andrews A B, Erskine J L, Kim K J and Harmon B N 1992 *Phys. Rev. Lett.* **68** 1931
[12] Sandratskii L M and Kübler J 1993 *Europhys. Lett.* **23** 661
[13] Nolting W, Dambeck T and Borstel G 1993 *Z. Phys.* B **90** 413
[14] Nolting W, Dambeck T and Borstel G 1994 *Z. Phys.* B **94** 409
[15] Li D, Pearson J, Bader S D, McIlroy D N, Walfried C and Dowben P A 1995 *Phys. Rev.* B **51** 13 895
[16] Weschke E, Schüßler-Langeheine C, Meier R, Fedorov A, Starke K, Hübinger F and Kaindl G 1996 *Phys. Rev. Lett.* **77** 3415
[17] Donath M, Gubanka B and Passek F 1996 *Phys. Rev. Lett.* **77** 5138
[18] Bode M, Getzlaff M, Heinze S, Pascal R and Wiesendanger R 1998 *Appl. Phys.* A **66** S121
[19] Getzlaff M, Bode M, Heinze S, Pascal R and Wiesendanger R 1998 *J. Magn. Magn. Mater.* **184** 155
[20] Bode M, Getzlaff M and Wiesendanger R 1998 *Phys. Rev. Lett.* **81** 4256
[21] Schüßler-Langeheine C, Weschke E, Mazumdar C, Meier R, Grigoriev A Yu, Kaindl G, Sutter C, Abernathy D, Grübel G and Richter M 2000 *Phys. Rev. Lett.* **84** 5624
[22] Stoner E C 1938 *Proc. R. Soc.* A **165** 372
[23] Slater J C 1936 *Phys. Rev.* **49** 537
[24] Slater J C 1936 *Phys. Rev.* **49** 931
[25] Sandratskii L M and Kübler J 1998 *Magnetism and Electronic Correlations in Local-Moment Systems: Rare-Earth Elements and Compounds* ed M Donath, W Nolting and P A Dowben (Singapore: World Scientific)
[26] Bode M, Getzlaff M, Kubetzka A, Pascal R, Pietzsch O and Wiesendanger R 1999 *Phys. Rev. Lett.* **83** 3017
[27] Bauer A, Mühlig A and Kaindl G 2001 *Phys. Rev.* B submitted
[28] Grübel G, Als-Nielsen J and Freund A K 1994 *J. Physique Coll.* **4** C9 27
[29] Weschke E, Schüßler-Langeheine C, Meier R, Kaindl G, Sutter C, Abernathy D and Grübel G 1997 *Phys. Rev. Lett.* **79** 3954
[30] Parratt L G 1954 *Phys. Rev.* **95** 359
[31] Deutsch M and Ocko B 1998 *Encyclopedia of Applied Physics* vol 23, ed G L Trigg and E H Immergut (Weinheim: Wiley–VCH)
[32] Warren B E 1969 *X-Ray Diffraction* (Reading, MA: Addison-Wesley)
[33] Helgesen G, Hill J P, Thurston T R, Gibbs D, Kwo J and Hong M 1994 *Phys. Rev.* B **50** 2990
[34] Weschke E, Schüßler-Langeheine C, Meier R, Kaindl G, Sutter C and Grübel G 1999 *Advances in Solid State Physics* vol 39, ed B Kramer (Braunschweig: Vieweg)
[35] Weschke E, Schüßler-Langeheine C, Meier R, Fedorov A V, Starke K, Hübinger F and Kaindl G 1996 *Surf. Sci.* **377–379** 487
[36] Li D, Zhang J, Dowben P A and Onellion M 1993 *Phys. Rev.* B **48** 5612
[37] Zhang J, Dowben P A, Li D and Onellion M 1995 *Surf. Sci.* **329** 177
[38] Kaindl G, Höhr A, Weschke E, Vandré S, Schüßler-Langeheine C and Laubschat C 1995 *Phys. Rev.* B **51** 7920
[39] Mulhollan G A, Garrison K and Erskine J L 1992 *Phys. Rev. Lett.* **69** 3240
[40] Weschke E and Kaindl G 1995 *J. Electron Spectrosc. Relat. Phenom.* **75** 233
[41] Meier R, Weschke E, Bievetski A, Schüßler-Langeheine C, Hu Z and Kaindl G 1998 *Chem. Phys. Lett.* **292** 507
[42] Schüßler-Langeheine C, Meier R, Ott H, Hu Z, Mazumdar C, Kaindl G and Weschke E 1999 *Phys. Rev.* B **60** 3449
[43] Schüßler-Langeheine C, Ott H, Grigoriev A Yu, Möller A, Meier R, Hu Z, Mazumdar C, Kaindl G and Weschke E 2001 *Phys. Rev.* B submitted
[44] Puglia C, Nilsson A, Hernnäs B, Karis O, Bennich P and Mårtensson N 1995 *Surf. Sci.* **342** 119
[45] Mårtensson N and Nilsson A 1995 *J. Electron Spectrosc. Relat. Phenom.* **75** 209
[46] Hong M, Flemings R M, Kwo J, Schneemeyer L F, Waszczak J V, Mannaerts J P, Majkrzak C F, Gibbs D and Bohr J 1987 *J. Appl. Phys.* **61** 4052
[47] Beach R S, Borchers J A, Matheny A, Erwin R W, Salomon M B, Everitt B, Pettit K, Rhyne J J and Flynn C P 1993 *Phys. Rev. Lett.* **70** 3502
[48] Ott H *et al* 2001 to be published
[49] Blume M and Gibbs D 1988 *Phys. Rev.* B **37** 1779
[50] Gibbs D, Grübel G, Harshman D R, Isaacs E D, McWhan D B, Mills D and Vettier C 1991 *Phys. Rev.* B **43** 5663
[51] Hannon J P, Trammell G T, Blume M and Gibbs D 1988 *Phys. Rev. Lett.* **61** 1245

[52] Gibbs D, Harshman D R, Isaacs E D, McWhan D B, Mills D and Vettier C 1988 *Phys. Rev. Lett.* **61** 1241
[53] Schüßler-Langeheine C, Weschke E, Grigoriev A Yu, Ott H, Meier R, Vyalikh D V, Mazumdar C, Sutter C, Abernathy D, Grübel G and Kaindl G 2001 *J. Electron Spectrosc. Relat. Phenom.* **114–116** 953
[54] Weschke E, Schüßler-Langeheine C, Mazumdar C, Meier R, Kaindl G, Sutter C and Grübel G 1998 *Magnetism and Electronic Correlations in Local-Moment Systems: Rare-Earth Elements and Compounds* ed M Donath, W Nolting and P A Dowben (Singapore: World Scientific)
[55] Carra P, Harmon B N, Thole B T, Altarelli M and Sawatzky G A 1991 *Phys. Rev. Lett.* **66** 5147
[56] Ahuja R, Auluck S, Johansson B and Brooks M S S 1994 *Phys. Rev.* B **50** 5147
[57] Langridge S, Paixão J A, Bernhoeft N, Vettier C, Lander G H, Gibbs D, Sørensen S A, Stunault A, Wermeille D and Talik E 1999 *Phys. Rev. Lett.* **82** 2187